Boundary-Layer Meteorol (2010) 136:193–218
DOI 10.1007/s10546-010-9507-y

ARTICLE

Energy Balance Closure Using Eddy Covariance Above Two Different Land Surfaces and Implications for CO_2 Flux Measurements

Joe Kidston · Christian Brümmer · T. Andrew Black · Kai Morgenstern · Zoran Nesic · J. Harry McCaughey · Alan G. Barr

Received: 5 September 2009 / Accepted: 4 March 2010 / Published online: 29 May 2010

Abstract Components of the surface energy balance of a mature boreal jack pine forest and a jack pine clearcut were analysed to determine the causes of the imbalance that is commonly observed in micrometeorological measurements. At the clearcut site (HJP02), a significant portion of the imbalance was caused by: (i) the overestimation of net radiation (R_n) due to the inclusion of the tower in the field of view of the downward facing radiometers, and (ii) the underestimation of the latent heat flux (λE) due to the damping of high frequency fluctuations in the water vapour mixing ratio by the sample tube of the closed-path infrared gas analyzer. Loss of low-frequency covariance induced by insufficient averaging time as well as systematic advection of fluxes away from the eddy-covariance (EC) tower were discounted as significant issues. Spatial and temporal distributions of the total surface-layer heat flux (T), i.e. the sum of sensible heat flux (H) and λE, were well behaved and differences between the relative magnitudes of the turbulent fluxes for several investigated energy balance closure (C) classes were observed. Therefore, it can be assumed that micrometeorological processes that affected all turbulent fluxes similarly did not cause the variation in C. Turbulent fluxes measured at the clearcut site should not be forced to close the energy balance. However,

J. Kidston · C. Brümmer · T. A. Black · K. Morgenstern · Z. Nesic
Faculty of Land and Food Systems, University of British Columbia, 2357 Main Mall, Vancouver, BC V6T 1Z4, Canada

Present Address:
J. Kidston
National Institute of Water and Atmospheric Research (NIWA), Wellington, New Zealand

C. Brümmer (✉)
Johann Heinrich von Thünen-Institut (vTI), Institute of Agricultural Climate Research (AK), Braunschweig, Germany
e-mail: christian.bruemmer@vti.bund.de; christian.bruemmer@ubc.ca

J. H. McCaughey
Department of Geography, Queen's University, Kingston, ON, Canada

A. G. Barr
Climate Research Division, Environment Canada, Saskatoon, Saskatchewan, Canada

at the mature forest site (OJP), loss of low-frequency covariance contributed significantly to the systematic imbalance when a 30-min averaging time was used, but the application of averaging times that were long enough to capture all of the low-frequency covariance was inadequate to resolve all of the high-frequency covariance. Although we found qualitative similarity between T and the net ecosystem exchange (NEE) of carbon dioxide (CO_2), forcing T to closure while retaining the Bowen ratio and applying the same factor to CO_2 fluxes (F_C) cannot be generally recommended since it remains uncertain to what extent long wavelength contributions affect the relationship between T, F_C and C.

Keywords Available energy flux · Eddy covariance · Energy balance closure · High-frequency loss · Latent heat flux · Low-frequency loss · Sampling-tube attenuation · Sensible heat flux · Turbulent flux cospectra

1 Introduction

The eddy-covariance (EC) technique is a powerful tool for measuring sensible heat, water vapour, and carbon dioxide (CO_2) fluxes between terrestrial ecosystems and the atmosphere over time scales of hours to years, and spatial scales of hundreds to thousands of m^2 (Wofsy et al. 1993; Schmid 1994; Baldocchi 2003, 2008). In combination with radiation and soil heat flux measurements, it provides detailed data to better understand the processes controlling ecosystem-atmosphere exchange (Law et al. 2002).

The evaluation of the surface energy balance closure (C) is an objective criterion in assessing data quality within the micrometeorological community (Aubinet et al. 2000; Wilson et al. 2002; Liu et al. 2006). The surface energy balance is closed when the energy flux into a system is equal to the energy flux leaving the system, plus any energy storage change in the system. At the Earth's surface this is expressed as

$$R_n = H + \lambda E + G + Q \tag{1}$$

where R_n is the net radiation flux density, H is the sensible heat flux density, λE is the latent heat flux density, G is the heat flux density into the soil surface, and Q is the sum of storage fluxes from any other energy sinks or sources, e.g., photosynthesis and change in the above-ground biomass heat storage (S_b). In our study, flux is, hereafter, an abbreviation for flux density. C is usually expressed as

$$C = \frac{H + \lambda E}{R_n - G - Q} \tag{2}$$

where the sum of the fluxes in the denominator is the available energy flux (A). We call the sum of the turbulent fluxes in the numerator the total surface-layer heat flux to which we assign the symbol T. Measurements of T are independent of those of A, so that C can be used to evaluate the relative accuracy of T versus A.

Analyses of numerous datasets obtained over various surface types have shown that T is often about 70–90% of A (Blanken et al. 1998; Aubinet et al. 2000; Twine et al. 2000; Wilson et al. 2002; Barr et al. 2006). Several explanations for this systematic imbalance have been hypothesized including different source locations for T versus A, measurement errors, neglected energy sinks, loss of low- or high-frequency contributions to the turbulent fluxes contained within T, and neglected transport processes of the surface-layer fluxes, e.g. horizontal and vertical advection and subsequent dissipation away from the EC tower due to processes not measured by EC

(Black et al. 1996; Mahrt 1998; Twine et al. 2000; Massman and Lee 2002; Wilson et al. 2002). With regard to the latter, Kanda et al. (2004) used large-eddy simulation (LES) to show that under convective conditions the flux magnitude in the surface layer is spatially heterogeneous due to convection cells. Lee and Black (1993) and Lee (1998) proposed that poor closure during unstable conditions was due to a non-zero mean vertical velocity. McNaughton (2004) described Theodorsen ejection amplifier-like structures, in which an initial ejection of air from near the ground into an ideal laminar and logarithmic flow induces vortical motion about a hairpin-shaped core. This creates a second ejection that is similar to, but larger than, the first, and may form at preferential locations such as edges or obstacles that distort flow and minor heterogeneities such as those with different albedo or roughness length (K. McNaughton, personal communication, 2006). It is unclear whether these vortical points would be at random or systematic locations, and what proportion of the excess transport at the vortex would be due to mass flow, which is not discernible by EC systems due to an inherent two- or three-dimensional nature (Finnigan 1999).

It is often assumed that the systematic imbalance is caused by the underestimation of the total heat flux T. Twine et al. (2000) demonstrated that, given the stated accuracy of the measurement of the components of A, their underestimation could not account for the magnitude of the imbalance. The authors argued that closure should be forced by increasing H and λE by keeping the measured Bowen ratio, i.e., $H/\lambda E$ is assumed constant. Wilson et al. (2002) highlighted that, for a given level of incident photosynthetically active radiation, reduced magnitudes of the measured NEE of CO_2 occurred during periods when the closure C was low. Reduced magnitudes of measured nocturnal NEE were found to coincide with low C. This is consistent with the hypothesis that variations in C are due to variations in how well the measurements of $H+\lambda E$ represent T, and that an underestimation of exchange might affect the measurement of all three surface-layer fluxes in a similar way.

Finnigan et al. (2003) demonstrated that, over tall canopy sites, loss of low-frequency covariance was a significant problem when 30-min averaging periods were used, and demonstrated similarity between T and NEE. A strong correlation between the closure and the friction velocity (u_*), atmospheric stability, and time of day was found by Barr et al. (2006) in three mature boreal forest stands in central Saskatchewan, Canada. Furthermore, they derived an analogous NEE closure fraction by normalizing the measured NEE against estimates from an empirical model that was tuned to high-u_* data, with this closure fraction responding similarly to u_*, atmospheric stability, and the time of day. Their results support the common practice of rejecting EC measurements during low-u_* periods and also lend support to the application of energy-closure adjustments to H, λE and NEE. However, results from open-path based EC fluxes measured over a black spruce forest in interior Alaska from Liu et al. (2006) suggested that $C < 1$ does not necessarily lead to an underestimation of CO_2 fluxes despite the existence of a surface energy imbalance. They showed that either an overestimation or underestimation of CO_2 fluxes is possible depending on local atmospheric conditions and measurement errors in H, λE, and the CO_2 flux.

The objectives of our study are as follows: (1) to determine the cause of the systematic underestimation in C by (a) investigating errors in the measurement of A, (b) quantifying the accuracy of the measurement of T by means of spectral analysis, and (c) assessing the temporal and spatial behaviour of T to qualify and quantify the occurrence of horizontal and/or vertical transport of surface layer fluxes; and (2) to determine whether NEE is underestimated when T is underestimated.

2 Basic Considerations

When conducting an energy balance study using eddy correlation, fluxes are not measured at the surface itself but for R_n, H, and λE (and NEE) across a plane at height h above the surface, and for G at depth d below the surface. Also the rate of change of energy storage between these two planes must be measured to conduct a full energy balance. In order to address the cause of the imbalance it is useful to define the measurements that make up the terms in Eq. 2.

Here, G is defined as

$$G = G_T + S_G \tag{3}$$

where G_T is the conductive heat flux measured by soil heat flux plates placed below the soil surface and S_G is the rate of heat storage change in the soil between the heat flux plates and the surface. Implicit in the definition of Eq. 3 is the assumption that there is no non-conductive transfer of heat across the plane of the heat flux plate, and that all energy storage change between the plate and the surface is sensible, i.e., phase change is ignored.

We express the total surface-layer heat flux as

$$T = (\lambda E_{\mathrm{EC}} + H_{\mathrm{EC}}) + (S_{\lambda E} + S_H) + (\lambda E_{\mathrm{other}} + H_{\mathrm{other}}), \tag{4}$$

where the first term on the right-hand side represents the turbulent flux at height h measured using the EC method, $\lambda E_{\mathrm{EC}} + H_{\mathrm{EC}} = T_{\mathrm{EC}}$, the second term is the rate of air-column storage change of the two scalars between the surface and h, and the third term is the transport across the plane at height h due to any non-turbulent flux process. Any divergence of upwelling longwave radiation between the surface and the EC height is included in the storage term in Eq. 4. Although this may result in slightly different magnitudes of H and λE, it does not affect C. This method of estimating H and λE was used since it is the best estimate of the surface values, and is also appropriate when discussing the similarity of surface-layer fluxes.

Systematic underestimation of T could result from the underestimation of the first and the second term on the right-hand side of Eq. 4, or if the third term is >0. The first term may be underestimated due to loss of high-frequency or low-frequency covariance resulting from sensor response or separation, averaging time or coordinate rotation. High-frequency loss can be corrected by applying a transfer function that depends on instrumentation, i.e., time constant, measurement frequency, path averaging, sensor separation, and flow rate in the tube of a closed-path infrared gas analyser (IRGA) as well as the actual turbulent cospectra at the site (Massman 2000). It may be possible to deal with low-frequency loss by extending the averaging time over which fluxes are calculated, but this also raises the possibility of the averaging time becoming so long that mean conditions are not stationary, and high-frequency deviations of scalar concentrations from the mean no longer accurately represent turbulent transport, thereby affecting the covariance with vertical wind speed (w).

In order to investigate whether the imbalance was caused by an overestimation of A or an underestimation of T, we first investigate the accuracy of A, then the accuracy of T_{EC}, i.e., $\lambda E_{\mathrm{EC}} + H_{\mathrm{EC}}$, before finally utilizing the temporal and spatial behaviour of T compared with A to draw conclusions on the likely magnitude of T_{other}. We use measurements from two long-term EC measurement sites with different surface characteristics, i.e., a clearcut and a mature forest, and also compare measurements from the long-term EC system in the clearcut with measurements from a second (auxiliary) system that was operated at different locations in the clearcut. The aim was to place the auxiliary system such that its flux footprint would lie within the same spatially homogeneous area as the main system footprint, and therefore the

true flux source strength for the two measurements would be the same. Furthermore, the second system was also placed away from the location of the main tower close to topographical features to investigate whether these might result in preferential signs of surface-layer fluxes at these points. At such a location, if some of the excess transport was turbulent, we would expect to find that C consistently exceeded C determined at the main tower. The advantage of doing this at a site with a long-term tower present is that we were able to obtain two datasets for C simultaneously and therefore variations in climatic conditions do not complicate the analysis of the spatial variation in C.

3 Methods

3.1 Description of Sites

The two sites used in this study are referred to as the Old Jack Pine (OJP) and Harvested Jack Pine 2002 (HJP02) sites and are part of a jack pine chronosequence within the BERMS (Boreal Ecosystem Research and Monitoring Sites) network (Zha et al. 2009). OJP, located approximately 100 km north-east of Prince Albert, Saskatchewan, Canada, near Narrow Hills Provincial Park, is a 79-year-old jack pine (*Pinus Banksiana* Lamb.) stand that is approximately 14 m tall with a range from 12 to 15 m (Kljun et al. 2006), a stand density of approximately 1190 trees ha^{-1} and a leaf area index (LAI) of 2.6 (Chen et al. 2006). EC flux measurements were made on a 30-m-tall steel scaffold tower at the 28-m height 3 m upwind of the tower. The 4-m-long air sampling tube to the infrared gas analyzer was heated and replaced twice a year. Net radiation was measured using upward and downward facing pyranometers (Model CM11, Kipp and Zonen, Delft, Netherlands) and pyrgeometers (Model PIR, The Eppley Laboratory Inc., Newport, Rhode Island, USA). The upward facing instruments were mounted at the top of the tower giving an unobstructed view of the sky and the downward facing instruments were mounted at the 24-m height 4 m south of the tower edge to minimize tower effects. Detailed site and instrumentation set-up information can be found in Baldocchi et al. (1997); Griffis et al. (2003) and Kljun et al. (2006). HJP02 (53.945° N, 104.649° W) is located approximately 4 km north-east of the OJP site (53.916° N, 104.692° W) at an elevation of 517 m above sea level. The site was logged in August 2000 and the surface was scarified in spring 2002. The ground cover consisted of common bearberry (*Arctostaphylos uva-ursi* (L.) Spreng), sparse grasses, sedges and reindeer lichen (*Cladina mitis* (Sandst.) Hustich) as well as slash left over from harvesting operations. Stand density before logging was likely similar to that at OJP. Post-harvest stump height was approximately 0.15 m with a diameter at this height of 0.15–0.20 m. The leftover slash formed patterned windrows (approximately 3 m wide with 4-m wide gaps between the windrows) up to 1 m high, which is characteristic of this type of harvesting operation. We therefore estimated the roughness length to be approximately 0.10 m (10% of the highest significant surface roughness elements), which was confirmed from the ratio of u_* to wind speed (U) in neutral conditions (0.11). The albedo of the site surface in the absence of a snow cover was approximately 0.15 ± 0.01 depending on volumetric soil water content (VWC), which had an annual mean of $0.12\,m^3\,m^{-3}$ for the 0–0.15 m layer when the soil was not frozen. The soil was a brunisol with sand, silt and clay fractions of 92, 6 and 2%, respectively, with organic matter visible only in the upper 0.10 m. The dominant vegetation types were bearberry, grasses and jack pine seedlings. LAI was determined by visually estimating the leaf area in several square sample plots and increased from 0.2 ± 0.2 to 0.5 ± 0.2 during the growing seasons of 2003–2005. The mean Bowen ratio during daytime hours with no snow cover in 2004 was 2.2 and varied from 4.9 during periods when the VWC

was in the lowest quintile to 0.97 when the VWC was in the highest quintile. A Lagrangian particle dispersion model (Kljun et al. 2002) was used to calculate the footprint contributions for x (direction parallel to the mean wind) and y (direction perpendicular to the mean wind). Different daytime scenarios, i.e. scenarios with variable H, U and stability, showed values of the longitudinal distance from the tower to the 90% cumulative flux footprint contour line between 70 and 130 m, which was less than the fetch in all directions for the main system location. For the nighttime scenario, it was 500 m, which was greater than the fetch in some directions, implying that under very stable conditions there may be a small contribution to the flux from beyond the clearcut. However, the wind direction at night was rarely from the south, which was the direction of minimum fetch, and nocturnal turbulent fluxes did not depend on wind direction, so these wind directions were not excluded.

3.2 Instrumentation at the HJP02 Site

The main tower was installed at the site in March 2003. High-frequency wind speed and air temperature (T_a) fluctuations at 2 m above the soil surface were measured with a 3-axis sonic anemometer-thermometer (model CSAT3, Campbell Scientific Inc. (CSI), Logan, Utah, USA) at a sampling frequency of 20 Hz. Water vapour and CO_2 density fluctuations were measured with an open-path IRGA (model LI-7500, LI-COR Inc., Lincoln, Nebraska, USA) from March 2003 to November 2003. In November 2003 a closed-path IRGA (model LI-7000, LI-COR Inc.) in a temperature-controlled housing to maintain its temperature at 37 ± 0.5°C was installed. A flow rate of at least 8 l min^{-1} ensured turbulent flow in the 2-m long sampling tube, which had an internal diameter of 4 mm. The IRGA was calibrated daily with dry N_2 (zero CO_2 and H_2O) gas and CO_2 standards from the Canadian Greenhouse Gases Measurement Laboratory of the Meteorological Service of Canada in Downsview, Ontario, Canada, with roughly atmospheric CO_2 concentration. Additional temperature and relative humidity measurements were made with a relative humidity probe (model HMP45C, Vaisala Oyj, Helsinki, Finland) mounted 1 m above the soil surface. Net shortwave radiation (R_{snet}) and net longwave radiation (R_{lnet}) were measured 2 m above the surface using a four-way radiometer (model CNR1, Kipp and Zonen).G_T was measured using four soil heat-flux plates (three model HFT3, Hukseflux, Delft, Netherlands) and one model CN3 (Middleton) (Carter–Scott Design, Melbourne, Australia) distributed radially about the tower at a depth of 0.03 m. S_G was computed from two temperature profiles, each with copper-constant thermocouples located at the 0.01-, 0.02- and 0.03-m depths. We assumed that the mean temperature in the top 0.03 m of the soil was $(3T_{0.01\ \mathrm{m}} + 2T_{0.02\ \mathrm{m}} + T_{0.03\ \mathrm{m}})/6$ in order to account for the non-linear soil temperature profile in the calculation of S_G. The VWC of the soil in the 0–0.15-m layer was measured using four soil water reflectometers (model CS615, CSI) distributed radially about the tower. U at the 5-m height was measured using a propeller-vane anemometer (model 05031, RM Young Co., Traverse City, MI, USA). The presence of surface water was measured using a leaf wetness sensor (model 237, CSI). Climate data were recorded with a data logger (model 23X, CSI) networked to a site computer, which also recorded digital (serial) signals from the sonic anemometer and IRGAs.

A second, auxiliary EC system, which was mounted on a tripod (model CM10, CSI) and was operated at different locations in the clearcut, was used for comparative measurements within the fetch of the main tower from August to October 2004. High-frequency water vapour and CO_2 density fluctuations were measured with a LI-COR Inc. LI-7500 IRGA. Wind speed and direction, relative humidity, R_{snet}, R_{lnet}, and G_T were determined using the same instruments at the same heights/depths as on the main tower. The VWC of the

soil was measured at 0.02–0.06 m and at 0.08–0.12 m below the surface using 2 CSI CS615 reflectometers, with all data recorded on a data logger (model CR5000, CSI).

3.3 Data Analysis

High-frequency IRGA water vapour and CO_2 densities were converted to the respective mixing ratios, m_w and m_c, and high-frequency IRGA and sonic anemometer signals were temporally aligned by maximizing the covariance of the IRGA signals with w. Due to the fact that the delay between the IRGA and the sonic signal did change, they were allowed to shift by up to 1 s. This was particularly important with the open-path IRGA because the delay depends on wind speed and direction more than for the closed-path IRGA, as the open-path IRGA was placed further than was the inlet to the sampling tube of the closed-path IRGA from the sonic array, and the delay varied depending on whether air passed first through the IRGA or the sonic arrays. The data were block-averaged over 30-min intervals and three rotations were performed on each averaging period so that the mean vertical ($\bar{w}$) and lateral ($\bar{v}$) velocity components, as well as the covariance between these velocity components ($\overline{w'v'}$), were zero (Tanner and Thurtell 1969). Here the prime indicates a fluctuation from the mean. The relationship between the rotated and non-rotated fluxes was the same for the locations of the auxiliary system as it was for the main location, being that the non-rotated flux was approximately 2% lower than the rotated flux. The small difference is expected when measurements are made close to a solid surface (Finnigan et al. 2003).

Outliers in the datasets of CO_2 and H_2O concentrations, T_a, U, radiation fluxes, and G, due to instrument malfunctions were removed, and where required the high-frequency time series was checked, before half-hourly fluxes were eliminated.

Daytime and nighttime measurements of R_n were removed if there was water on the upward-facing pyrgeometer windows as indicated by the wetness sensor. This was necessary because the wetting of the sensor windows caused the difference between the longwave radiation incident upon and emitted from the pyrgeometer sensing surface to tend to zero. Data were also removed at night when $A > 0$, since systematically low C during these half-hours was likely caused by a thin layer of condensation, resulting in spuriously low magnitude R_n measurements.

At both sites, turbulent fluxes were removed when the wind direction was $>45°$ and $<135°$ from north, as the closure C was systematically low for these wind directions. This was likely due to flow distortion caused by the airflow passing through the tower before encountering the EC instrumentation—the EC instrumentation was installed on the west facing side of the tower at both sites.

For a given time interval, C was calculated using three methods. The first was to calculate the slope of the regression using the ordinary least squares of T against A (OLS method). In the second and third methods, the mean of the ratio of T to A (MOR method), and the ratio of the mean of T to the mean of A (ROM method), were determined respectively.

Turbulent cospectra were calculated for w and T_a as well as w and m_w. Where different averaging times were used, the high-frequency data were amalgamated into a continuous time series for each respective trace before the cospectra were processed. The respective traces were linearly detrended and filtered using a Hamming window before the covariance was calculated for 100 logarithmically increasing frequency ranges and then averaged to 25 frequency ranges for the spectral plots.

4 Results and Discussion

4.1 Accuracy of the Measurement of the Available Energy A

4.1.1 Net Radiation at the HJP02 Site

Sources of error in measurements can be split into (a) calibration and (b) physical errors. Following Twine et al. (2000), calibration errors were discounted as sources of the systematic imbalance. The latter are caused by climatic effects on radiometers, possible unfavourable instrument design, voltage measurement errors, and any systematic spatial heterogeneity between the footprints of R_n and T, which may arise from (i) true spatial variability of the site in question, and (ii) inclusion of the tower in the field-of-view of the net radiometer. Spatial variability at the site is also discounted as the cause of the systematic imbalance because, across multiple sites, this is a random error and therefore does not produce a systematic imbalance (Twine et al. 2000; Wilson et al. 2002). Furthermore, good agreement has been found between multiple instruments deployed at the same site (this study, data not shown; Twine et al. 2000). Weather effects on radiometers, however, as given in the specifications of the CNR 1 radiometer employed at HJP02 can cause errors in the range of -15 to $+25\,\mathrm{W\,m^{-2}}$. Firstly, as a result of the cooling of the silicon window on the upward facing pyrgeometer at night because it has a higher thermal emissivity than that of the air between the window and the sensor surface. Secondly, because of the heating of this window due to absorption of shortwave radiation during daytime.

Furthermore, the measurement of R_n may be biased by the inclusion of the mounting tower in the field-of-view. The main tower at HJP02 was constructed of galvanized steel, with albedo (a) and thermal emissivity (ε) both estimated to be approximately 0.3 (http://www.uppco.com). The radiometer's field-of-view occupied by the tower was calculated to be approximately 5% taking into account the size and distance of beams and cross beams. Consequently, the albedo and emissivity of the field-of-view of the downward facing pyranometer and pyrgeometer measurement are given by

$$a_{\mathrm{FOV}} = 0.95a_g + 0.05a_t, \tag{5}$$

$$\varepsilon_{\mathrm{FOV}} = 0.95\varepsilon_g + 0.05\varepsilon_t, \tag{6}$$

where the subscripts g and t refer to the ground and tower, respectively.

Given that we measured a_{FOV} to be 0.15, Eq. 5 can be rearranged to give $a_g = 0.142$, and so the inclusion of the tower in the field-of-view caused a_{FOV} to be 5.5% higher than a_g. For a typical sunny midday situation, the measurement of upwelling shortwave radiation (R_{su}) equalling $75\,\mathrm{W\,m^{-2}}$ is an overestimation by 5.5%, or $5\,\mathrm{W\,m^{-2}}$. Assuming $\varepsilon_g = 0.95$ (Campbell and Norman 1998) (Eq. 6), $\varepsilon_{\mathrm{FOV}}$ becomes 0.918, so the inclusion of the tower in the field-of-view caused $\varepsilon_{\mathrm{FOV}}$ to be 3.5% lower than ε_g. Assuming that due to the small diameter of the tower bars and high clearcut wind speeds, i.e. high boundary-layer conductance, there was efficient exchange of sensible heat between tower surfaces and the atmosphere, the tower is approximately at air temperature. The air and the tower would actually be cooler than the ground, but for simplicity we assume they are in thermal equilibrium, implying that reduced thermal emissivity resulted in a reduced upwelling longwave radiation (R_{lu}), whence R_{lu} was underestimated by $\approx$3.5%, or $\approx 16\,\mathrm{W\,m^{-2}}$ for a typical midday situation. This also shows that the emissivity difference between the tower and the ground has a much greater effect than the temperature contrast. The errors in the upwelling radiative fluxes due to the inclusion of the tower in the field-of-view, as well as those specified in the CNR 1 manual

(http://www.kippzonen.com) imply that for a typical midday situation, R_n is systematically overestimated by 31 W m^{-2} or 10%, not taking any random components into account.

Measurements of longwave radiation at night may also have a bias related to the warming or cooling of the window covering the upward or downward-facing pyrgeometers. At OJP, an Eppley Laboratory (Newport, Rhode Island, USA) model PIR pyrgeometer (Barr et al. 2006) was used to measure longwave downwelling radiation (R_{ld}), which includes a measurement of the temperature of the window as well as the pyrgeometer sensor temperature. The window was generally cooler than the sensor surface at night, and so the nocturnal correction was positive with a magnitude of up to 5 W m^{-2}. Given that the mean of the nocturnal A at HJP02 when conditions were considered ideal was -27 W m^{-2}, and the nocturnal C under such conditions was approximately 90%, it is possible that a correction to R_{ld}, would increase the nocturnal C to unity.

This analysis indicates that the error in R_n due to the inherent physical errors associated with making the measurement may be of the appropriate sign and magnitude to be responsible for a significant proportion of the observed imbalance during daytime, and suggests that this may also be the case at night. Regardless of the accuracy of the instrument, inclusion of the tower in the field-of-view introduces systematic heterogeneity between the field-of-view of A and the footprint of T, thus it cannot be expected that C equals 100%. These errors need to be addressed on a site-by-site basis, accounting for specific instrumentation and tower geometry, before the turbulent fluxes might defensibly be forced to obtain closure.

4.1.2 Diurnal Variation of the Surface Energy Balance Closure: Implications for the Accuracy of the Energy Storage Fluxes

Another approach to examining the accuracy of the available energy A was to analyze systematic features in the diurnal variation of C, which is shown for the months of June 2003,

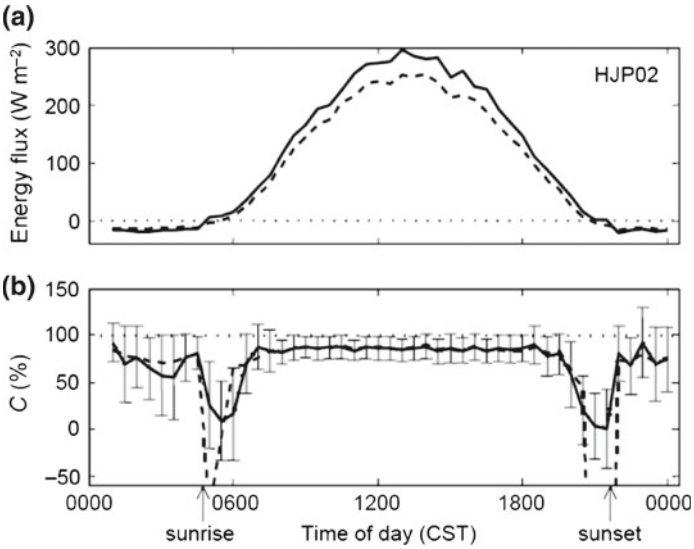

Fig. 1 **a** Ensemble averages ($n = 90$) of $R_n - G$ (available energy flux, A, *solid line*) and $H + \lambda E$ (total surface layer heat flux, T, *dashed line*) for the HJP02 site during June 2003, 2004, and 2005. **b** Mean of energy balance closure (C) for each half-hour period (MOR method, i.e. the mean of the ratio of T to A, *solid line*) with *error bars* representing 1 standard deviation for each half-hour as well as the ratio of the mean of T to the mean of A (ROM method, *dashed line*)

2004, and 2005 at HJP02 in Fig. 1. A physical explanation for the dip in C during sunrise and sunset, which was observed throughout the year, is likely explained as follows. As can be clearly seen in the ROM method, during these periods average A was positive and average T was negative or close to zero. R_n was negative, as was G, but with a larger magnitude, and the sun was above the horizon [as detected from the potential, i.e., clear-sky, downwelling shortwave radiation (R_{sdpot}), calculated assuming constant atmospheric transmissivity (0.80) from Stull (1998)]. When the sun's zenith angle was large, the amount of energy penetrating the above-ground biomass and debris likely became decoupled from G due to the fact that the angle of incidence remained low for much of the above-ground biomass. At these times, there would be a disproportionately greater heat flux going into the above-ground biomass than the soil surface even if G were negative. At HJP02, S_b was not measured, but it would have made Q less negative during these periods. Hence, A would be negative or closer to zero, which would increase C. During the rest of the diurnal cycle this was less significant because (i) S_b was in phase with S_G, and (ii) $S_G + S_b$ was a relatively small percentage of A. If the ensemble average diurnal C were plotted for the entire summer, mean daily C would be lower due to this effect for longer periods in the morning and afternoon because the length of these periods would vary considerably. The fact that S_G, S_b, S_H, and $S\lambda_E$ are approximately 90° out of phase with the rest of the energy fluxes, i.e., the storage fluxes were positive in the morning, but negative throughout the afternoon, implies that the diurnal variation of C allows a qualitative analysis of the accuracy of the sum of the storage fluxes. This is because C would systematically decrease throughout the daytime if these fluxes were underestimated, and increase if they were overestimated (assuming that a possible physical underestimation of T was not dependent on time of day). The fact that C remains constant throughout the daytime (excluding sunrise/sunset) is therefore a strong indication that S_G was well measured at HJP02.

Standard deviations for a given half-hour MOR value were higher during nighttime and sunrise/sunset than during the day. This is because (a) fluxes were close to zero, and (b) turbulence can be intermittent at night (Stull 1998), and measured turbulent fluxes are dependent on the turbulence intensity. The former means that the ratio for individual half-hours can be large, giving a high standard deviation. The dataset can become skewed due to this effect to the extent that the MOR method no longer accurately represents the average C. Therefore, limits were set for the MOR method, i.e. individual half-hours with $C < -100$ and $C > 200\%$ were excluded.

The diurnal variation of C at the OJP site is shown in Fig. 2. C consistently increased throughout the day. Given that this behaviour is not in phase with the variation of any of the climatic variables that dictate the state of the surface layer (e.g., R_{sd}, relative humidity, and u_*), one possible explanation is that the energy storage change between the ground and the EC measurement height was underestimated. Another reason might be that mesoscale circulations became established in the afternoon. A factor of 1.5 applied to S_H and $S\lambda_E$, and a factor of 2 applied to S_b made C constant throughout the day. However, at OJP the standard deviation for a given MOR value during daytime was higher than at HJP02 (Fig. 1), which indicates that distinctly different processes influenced the variation of C at the two sites.

This analysis supports the assumption that a systematic diurnal variation of C at both HJP02 and OJP sites was likely partly due to the accuracy of the measurement of the storage fluxes, i.e. the underestimation of S_b, contained within A at sunrise and sunset at HJP02, and throughout the daytime at OJP. If closure is analyzed for dependencies using 1:1 plots of half-hour flux values, spurious relationships are found because climatic variables such as R_{sd}, relative humidity, u_*, and surface-layer stability all exhibit a systematic diurnal

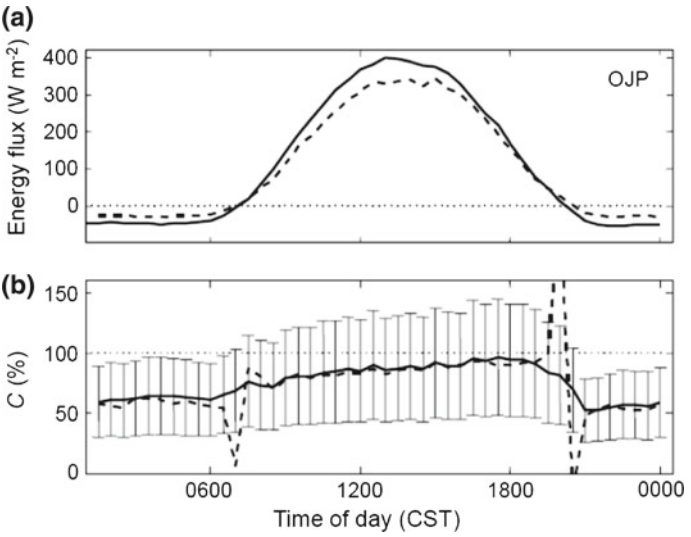

Fig. 2 **a** Ensemble average of A (*solid line*) and T (*dashed line*). Data were recorded at the OJP site between day of year (DOY) 150–300, 2004 and 2005. **b** C using the MOR method (*solid line*) with *error bars* representing 1 standard deviation as well as C using the ROM method (*dashed line*)

variation. Analyzing C for dependency using either a ensemble-average diurnal variation or daily values bypassed this problem.

In addition, we considered the dependency of C on the atmospheric stability parameter $\xi = z/L$, where z is measurement height and L is the Obukhov length. The calculation of ξ is affected when H and λE are forced to closure. Hence, it is likely that the use of z/L would result in spurious dependencies being found. Thus, if, for example, H or λE is underestimated, L would be overestimated, thereby underestimating ξ, which would lead to a spurious positive correlation between C and ξ. Furthermore, if total energy T and NEE were forced to closure on a half-hourly time scale, NEE would be biased due to the fact that NEE revealed diurnal variations and therefore a large correction factor would be applied in the morning. At this time of the day NEE can be more negative than in the afternoon as a result of conditions being more conducive for photosynthesis.

4.2 Accuracy of the Measurement of T_{EC}

4.2.1 Underestimation of High-Frequency Contributions to λE_{EC}

One method of estimating the high-frequency loss of λE_{EC} is to calculate a water vapour flux transfer function (TF_{H_2O}) using ensemble-average wm_w and wT_a cospectra. An unnormalised TF_{H_2O} ($TF^{UN}_{H_2O}$) was calculated as the ratio of the unnormalised wm_w cospectra to the unnormalised wT_a cospectra multiplied by $\rho_a \lambda / \rho c_p$, where ρ_a is the dry air density, λ is the latent heat of vaporisation, ρ is the air density and c_p is the specific heat of air. The $TF^{UN}_{H_2O}$ was then normalized by the value of $TF^{UN}_{H_2O}$ at a subjectively chosen frequency (f_1), below which it was assumed that no high-frequency degradation occurred. The underestimation of λE_{EC} was calculated as the ratio of the integral over the entire frequency range of the wT_a cospectrum multiplied by TF_{H_2O}, to the integral of the wT_a cospectrum over the same frequency range without TF_{H_2O} applied. Since the loss of high-frequency covariance in the wm_w

Table 1 Summary of the underestimation of λE_{EC} due to high-frequency attenuation of H_2O variance by the sample tube of the closed-path IRGA

Site	Relative humidity stratification	u_* Stratification	F_1 (Hz)	Underestimation of λE_{EC} (%)
HJP02	Low	Low	0.30	5
	Low	High	0.30	8
	High	Low	0.050	24
	High	High	0.050	31
OJP	Low	Low	0.60	0
	Low	High	0.60	2
	High	Low	0.40	0
	High	High	0.40	3
	High	Low	0.060	3
	High	High	0.060	12

Transfer functions (TF) were calculated based on the data shown in Fig. 3a (HJP02 site) and Fig. 3b (OJP site) for the low and high relative humidity stratifications, and set to unity below frequency f_1. Underestimation of λE_{EC} is calculated as the difference from unity of the ratio of the integral of the wT_a cospectra over all frequencies with the appropriate TF applied, to the integral of the wT_a cospectra over all frequencies without the TF applied. The wT_a cospectra for the high and low u_* stratifications are shown in Fig. 4a (HJP02) and Fig. 4b (OJP)

cospectra results in incorrect normalization factors being applied when individual cospectra are first normalized by the total covariance for the time period, we decided to use unnormalised cospectra. Ensemble-average cospectra become distorted due to a range of incorrect normalization factors. Implicit in this analysis is the assumption of spectral similarity between the surface-layer fluxes at high frequency (Stull 1998). Hence, the high-frequency degradation of the wm_w cospectra relative to the wT_a cospectra is attributed to a slower system response of the closed-path IRGA relative to the sonic anemometer-thermometer.

Figure 3a shows $TF^{UN}_{H_2O}$ for the closed-path IRGA at HJP02 for three relative humidity stratifications. Data were recorded during July 2004 when $H > 100\,W\,m^{-2}$ and $\lambda E > 75\,W\,m^{-2}$. The correlation of $TF^{UN}_{H_2O}$ at low frequency with relative humidity is due to the correlation of the Bowen ratio with relative humidity, i.e., when relative humidity is high, the Bowen ratio is low. The reduction of the ratio of the cospectra at high frequency indicates that λE_{EC} exhibits high-frequency degradation at all relative humidity stratifications and appears to begin at lower frequencies when relative humidity is high. For low and for high relative humidities, f_1 is assumed to be 0.3 and 0.05 Hz, respectively. This selection, although being somewhat subjective, is justified by the fact that there is not necessarily spectral similarity for the surface-layer fluxes at low frequency due to different source locations and that there is more variation in the cospectra at low frequencies because the spectral bins contain fewer points.

Figure 3b shows $TF^{UN}_{H_2O}$ for data recorded at the OJP site. $TF^{UN}_{H_2O}$ shows less variation in the low frequency for the relative humidity stratifications, indicating that the Bowen ratio is not as strongly correlated with relative humidity at OJP as it is at HJP02. $TF^{UN}_{H_2O}$ shows a similar reduction at high frequency as occurs at HJP02, indicating qualitatively similar high-frequency degradation of λE_{EC}. As for HJP02, the choice of f_1 is subjective, particularly for the high relative humidity stratification (Table 1).

The impact that a given transfer function has on the measured covariance depends on what proportion of the true covariance lies above f_1. Figure 4a shows the wT_a cospectra for the same half-hours as shown in Fig. 3a, but stratified by u_*. The cospectra are unnormalised,

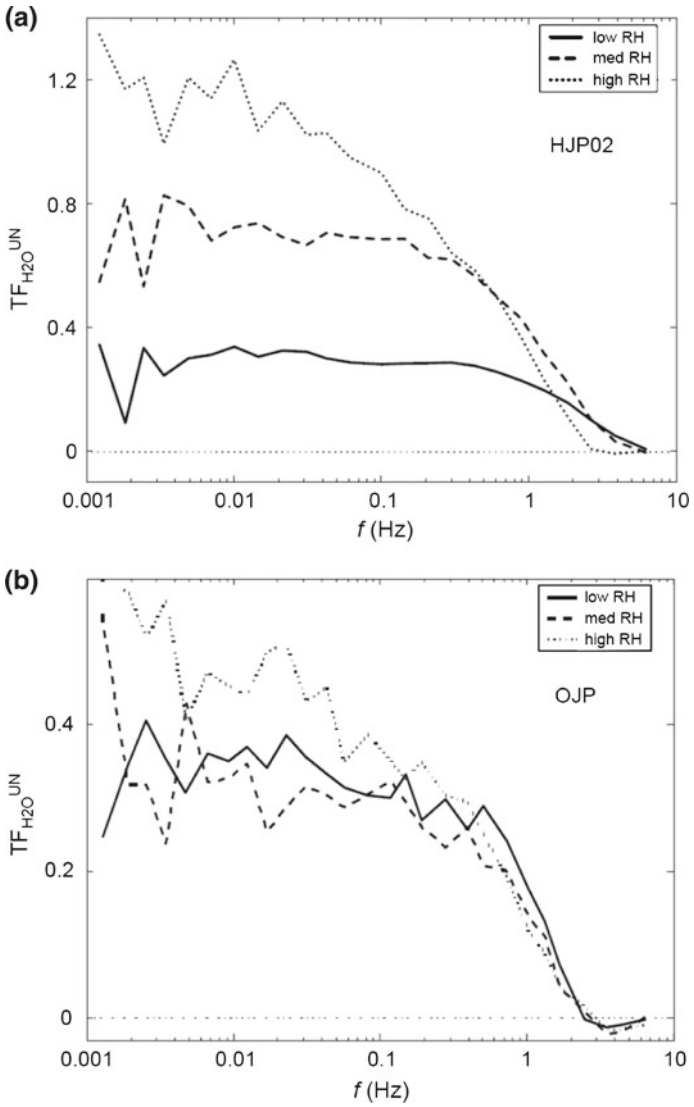

Fig. 3 **a** Ratio of ensemble average vertical wind speed and H_2O mixing ratio (wm_w) cospectra to wT_a cospectra, stratified by relative humidity (RH) with RH < 30% (*solid line*), 50% < RH < 57% (*dashed line*), and 60% < RH (*dotted line*). Data were recorded during July 2004 at HJP02 when $H_{EC} > 100\,W\,m^{-2}$, $\lambda E_{EC} > 75\,W\,m^{-2}$, and CO_2 flux measured by the EC instrumentation (F_C) > 0. The number of half-hour periods contained within the low, medium, and high RH stratifications is 22, 20, and 18, respectively, and the mean RH for the low, medium, and high RH stratifications is 26, 53, and 72%, respectively. **b** Ratio of ensemble average wm_w mixing ratio cospectra to wT_a cospectra, stratified by RH with RH < 40% (*solid line*), 42% < RH < 48% (*dashed line*), and 60% < RH (*dotted line*). Data were recorded during July and August 2003 at OJP when $H_{EC} > 150\,W\,m^{-2}$, $\lambda E_{EC} > 100\,W\,m^{-2}$, and $F_C < -5\,\mu mol\,m^{-2}\,s^{-1}$. The number of half-hour periods contained within the low, medium, and high RH stratifications is 21, 19, and 21, respectively, and the mean RH for the low, medium, and high RH stratifications is 35, 45, and 68%, respectively

so that the area under the curve represents the total covariance or kinematic flux. Relative to the wT_a cospectrum for all u_*, there is a greater proportion of high-frequency transport when u_* is high and less when it is low due to the effect that half-hour periods of high u_* correspond to half-hours with high U. For these approximately similar climatic conditions, half-hour periods with low u_* correspond to more unstable conditions, which tend to exhibit a greater proportion of low-frequency transport (Finnigan et al. 2003).

The wT_a cospectra for the same half-hour periods that are shown in Fig. 3b for OJP are shown in Fig. 4b. At OJP the wT_a cospectrum peaks at lower frequencies than at HJP02. Although there is a qualitatively similar shift to high/low frequencies during high/low u_* periods, the proportion of transport at frequencies above f_1 is lower at OJP than at HJP02. Hence, the transfer functions calculated for OJP have less impact than for HJP02. The underestimation of λE_{EC} found during the half-hour periods when u_* is both high and low is summarised in Table 1.

This analysis indicates that underestimation of λE_{EC} due to the attenuation of high-frequency m_w variance is significant, particularly at HJP02, where f_1 is closer to the spectral peak than at OJP. The impact on C would depend on the particular transfer function that was in effect, the content of the true wm_w cospectrum, and the Bowen ratio during the measurement period. Similar analysis for the CO_2 flux (F_C) indicates that there is high-frequency degradation of F_C relative to H_{EC}. However, the magnitude of the loss is not correlated with relative humidity because the transfer function for CO_2 ($\mathrm{TF}_{\mathrm{CO_2}}$) is not relative humidity dependent.

The results presented in Table 1 leads one to suspect that the systematic imbalance at HJP02 is entirely due to high-frequency degradation of λE_{EC}. This was further investigated by plotting C as a function of the ratio of λE_{EC} to H_{EC} (Fig. 5). For approximately similar weather conditions, i.e., $R_{\mathrm{sdpot}} > 500\mathrm{W\ m^{-2}}$, C decreases as the ratio of λE_{EC} to H_{EC} increases. However, if the imbalance is entirely due to an underestimation of λE_{EC}, C would equal unity when the true λE is zero. Visual extrapolation of this graph indicates C is approximately 90% when $\lambda E = 0$. Hence, even when λE is very small, a systematic imbalance persists, which is of the appropriate magnitude as to be consistent with the overestimation of R_n proposed in the previous section. The imbalance also persists at night when λE is close to zero. Similar results were found by Barr et al. (2006) who demonstrated that λE was the strongest contributor to C at a 70-year-old and 21-m tall aspen stand (known as Old Aspen) in Saskatchewan, Canada. They found that C was 0.91 when the evaporative fraction, i.e. $\lambda E/(\lambda E + H)$, was close to zero and was ≈0.86 when the evaporative fraction was 0.7, indicating that the λE contribution to turbulent heat/energy exchange was more than twice as high as the H contribution.

4.2.2 Loss of Low-Frequency Covariance Due to Insufficient Averaging Time

In the process of computing fluxes, averaging times that are too short lead to a loss of low-frequency covariance and tend to reduce the magnitude of the flux. Finnigan et al. (2003) presented data where increasing the averaging and coordinate rotation period to 4 h increased C to 100%. The wT_a cospectra for HJP02 (Fig. 4a) and OJP (Fig. 4b) show marked differences at low frequencies. At HJP02, the covariance falls to zero at low frequency ($f < 0.002$) and the cospectra more closely approaches zero when 100 frequency ranges are retained, indicating that the 30-min averaging time is sufficient to capture most of the low-frequency covariance. At OJP, however, the cospectra do not fall to zero at low frequency ($f < 0.002$) for both the low and all-u_* stratifications, indicating that surface-layer fluxes are underestimated due to insufficient averaging time. When u_* is low or average at OJP, there is

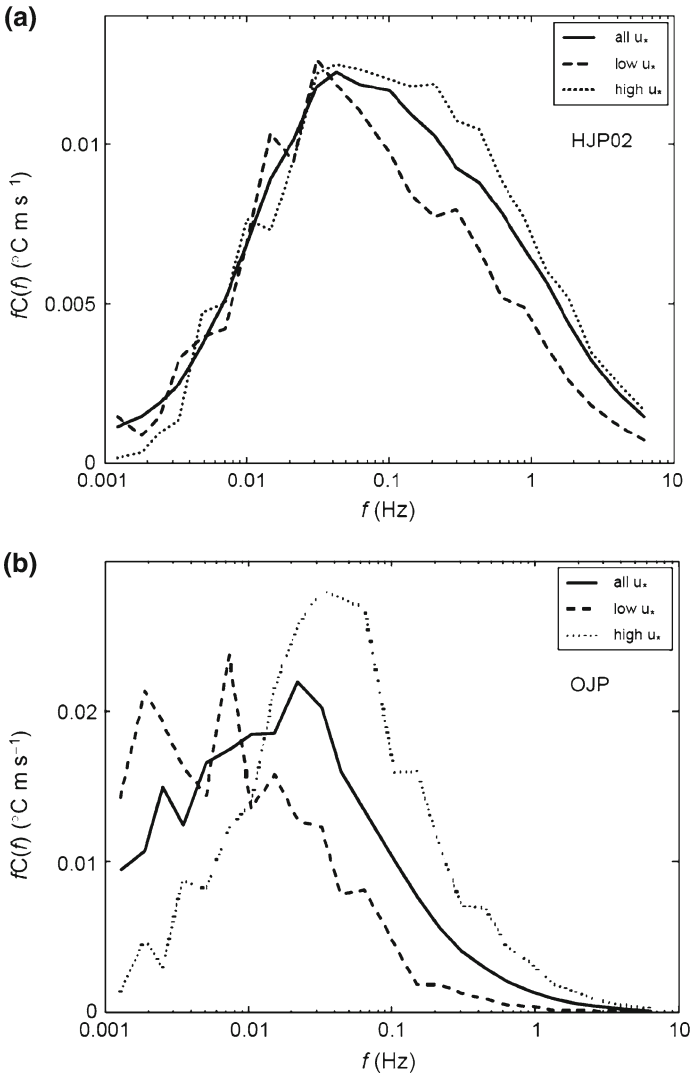

Fig. 4 **a** Ensemble average wT_a cospectra stratified by friction velocity (u_*) with $u_* < 0.4\,\mathrm{m\,s^{-1}}$ (*dashed line*), all u_* (*solid line*), and $u_* > 0.7\,\mathrm{m\,s^{-1}}$ (*dotted line*). Data were recorded at HJP02 during the same half-hour periods as the data shown in Fig. 3a. The low-, all-, and high-u_* stratifications contain 13, 153, and 18 half-hour periods, respectively. **b** Ensemble average wT_a cospectra stratified by u_* with $u_* < 0.4\,\mathrm{m\,s^{-1}}$ (*dashed line*), all-u_* (*solid line*), and $u_* > 1.1\,\mathrm{m\,s^{-1}}$ (*dotted line*). Data were recorded at OJP during the same half-hours as the data shown in Fig. 3b. The low-, all-, and high-u_* stratifications contain 10, 109, and 9 half-hour periods, respectively

significant covariance at periods longer than 30 min. Thus, T_{EC} was underestimated due to a loss of low-frequency covariance. The fact that the low-frequency loss has a greater impact on the underestimation of T_{EC} than the high-frequency degradation of λE_{EC} is consistent with the positive correlation between C and u_* during the daytime at the OJP site (Barr et al. 2006). Considering the cospectral content shown in Fig. 4b, this would be expected, since it

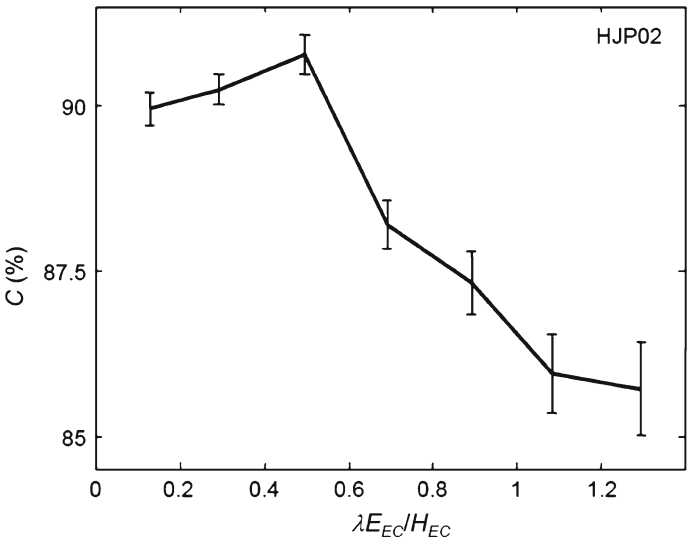

Fig. 5 Energy balance closure (C) as a function of $\lambda E_{\mathrm{EC}}/H_{\mathrm{EC}}$. Data were recorded at HJP02 between May and September 2004 and 2005 when clear-sky downwelling shortwave radiation (R_{sdpot}) $> 500\,\mathrm{W\,m^{-2}}$ and have been bin averaged by $\lambda E_{\mathrm{EC}}/H_{\mathrm{EC}}$. Also shown is the standard error of the mean for each bin

Table 2 Regression parameters for T_{EC} computed using longer averaging periods against T_{EC} computed using a 30-min averaging period

Site	Averaging time (min)	Slope[a,b]	Intercept[a,b]	n	R^2	RMSE ($\mathrm{W\,m^{-2}}$)
HJP02	60	1.00 (0.98, 1.03)	0.74 (0.43, 1.06)	535	0.97	9.32
	120	0.98 (0.96, 1.00)	3.62 (1.96, 5.28)	266	0.95	9.71
OJP	60	1.04 (1.03, 1.05)	−0.09 (−1.68, 1.50)	1331	0.98	26.85
	120	1.07 (1.06, 1.08)	−1.80 (−5.05, 1.65)	664	0.96	35.23
	240	1.10 (1.08, 1.13)	4.15 (−0.12, 8.42)	326	0.92	47.31

The 30-min fluxes are averaged over 2, 4, or 8 periods, for comparison with the 60-min 120-min and 240-min fluxes, respectively. Regressions include data for the entire diurnal cycle. Data were recorded during July 2004 at HJP02 and during July and August 2003 at OJP

[a] e.g. $T_{\mathrm{EC\ 60\ min}} = \mathrm{Slope} \times T_{\mathrm{EC\ 30\ min}} + \mathrm{Intercept}$

[b] 95% confidence bounds are given in parentheses

appears that the full low-u_* cospectra have a greater contribution at frequencies $<10^{-3}$ Hz than do the high-u_* cospectra have above f_1.

In order to confirm that the 30-min averaging time is sufficient at HJP02 and to quantify the underestimation of T_{EC} due to loss of low-frequency covariance at OJP, EC fluxes for both sites were calculated using longer averaging periods. Table 2 presents regression parameters for T_{EC} computed using these longer averaging periods (60, 120 and 240 min) against T_{EC} computed using a 30-min averaging period. As expected from the low-frequency content of the wT_a cospectra, longer averaging periods do not increase T_{EC} at HJP02. Conversely, at OJP, T_{EC} increased as the averaging period increased. When linearly detrended fluxes were compared, the effect of increased averaging periods is similar, but the slopes of the regression are approximately 2% lower.

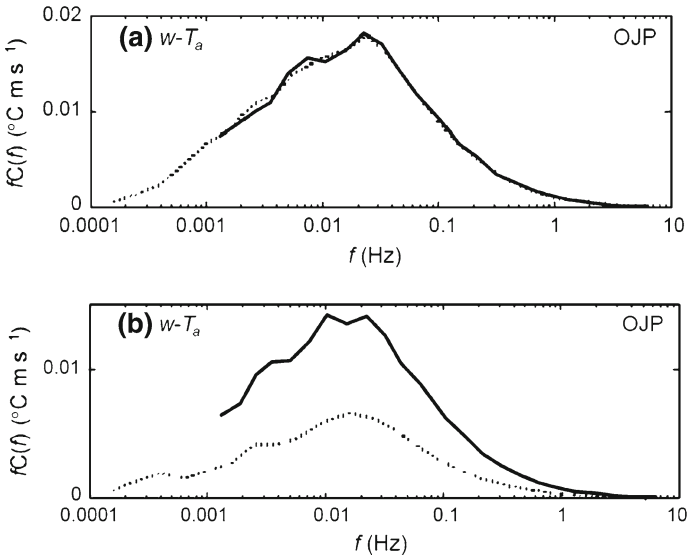

Fig. 6 **a** Ensemble-averaged wT_a cospectra for an averaging period of 30 min (*solid line*) and an averaging period of 240 min (*dotted line*). Data were recorded at OJP between 1000 and 1400 CST during July and August 2003. **b** Ensemble average wT_a cospectra for an averaging period of 30 min (*solid line*) and an averaging period of 240 min (*dotted line*). Data were recorded at OJP between 0600 and 1000 CST during July and August 2003

Figure 6a compares the ensemble-averaged wT_a cospectra obtained for the period between 1000 and 1400 CST at OJP during July and August 2003 for 30-min and 240-min averaging periods, plotted so that the area under the curve represents the kinematic flux. It is clear from the low-frequency content of the cospectra that the 30-min averaging period is insufficient, and that an averaging period of 240 min is required to recover the low-frequency covariance. When the cospectra for the 60- and 120-min averaging periods are included, they terminate progressively closer to zero in the low-frequency range. When HJP02 data are analyzed similarly, the cospectra fall to zero at low frequency ($f < 0.002$) regardless of the averaging time, verifying that a 30-min period is sufficient. These results provide a qualitative explanation for the increase of T_{EC} with averaging time at OJP. Quantitative consistency is indicated by the fact that the kinematic flux for the 30-min averaging period was 90 and 87% of the kinematic flux for the 240-min averaging period for H_{EC} and λE_{EC}, respectively. This is consistent with the slope of 1.10 given in Table 2 for the regression of T_{EC} calculated using a 240-min averaging time against T_{EC} calculated using an averaging time of 30 min.

The increased T_{EC} at OJP for longer averaging periods results in C increasing to a maximum of 90% for the 240-min averaging time. The remaining imbalance is likely not an artefact of insufficient averaging time because, during the period 1000–1400 CST, 240-min appears to be sufficient to recover all of the low-frequency covariance (Fig. 6a). Also, the underestimation of λE_{EC} due to high-frequency attenuation of H_2O variance likely does not account for such a large imbalance. No nocturnal u_*-threshold (u_*^{th}) was applied to the data before calculating the OLS closure because the validity of comparing 240-min fluxes with non-contiguous 30-min fluxes is questionable, but such a treatment may have increased C for all averaging periods. However, it is also likely that when longer averaging periods are

used, conditions are non-stationary within the averaging period, reducing the covariance, and therefore C is reduced when the regression includes fluxes from all times of the day.

An analysis similar to that shown in Fig. 6a but for data recorded between 0600 and 1000 CST is shown in Fig. 6b. The 30-min cospectra do not fall to zero at low frequency, implying that a 30-min averaging time is insufficient to capture the low-frequency covariance. The 240-min cospectra did, however, fall to approximately zero at low frequency, but relative to the 30-min cospectra, the covariance is reduced at all frequencies. High frequency deviations of scalar concentration from the mean (or linearly detrended) values during non-stationary conditions are not representative of physical transport phenomena. This may imply that during these periods, such as the early morning, the averaging time required to capture all of the low-frequency covariance is necessarily too long to retain the high-frequency covariance, consequently EC fluxes cannot represent the true ecosystem-atmosphere exchange in such circumstances. However, this only applies when using the simple covariance for determining the flux, since it is theoretically possible to obtain the flux for periods shorter than the maximum wavelength when the flux is computed as an integral of the wavelet cross-scalogram, as presented by Mauder et al. (2007). Although we found similarity between the wT_a and wm_w cospectra at the OJP site during such conditions, we do not recommend forcing the turbulent fluxes to closure, since it is not clear whether the individual fluxes behave in the same way.

This result places an onus on the need for the highest possible accuracy in the available energy A and particularly the storage fluxes. They are out of phase with R_n, T_{EC} and NEE. If the closure-based correction factors have a magnitude that varies with the magnitude of the surface-layer fluxes, C would be systematically low in the morning and high in the evening, thereby biasing long-term sums.

4.3 Spatial and Temporal Variability of Surface-Layer Fluxes at HJP02

4.3.1 Implications for the Occurrence of Systematic Horizontal and/or Vertical Transport of Surface-Layer Fluxes

Different measurement locations were chosen to test the hypothesis that the energy imbalances at HJP02 are due to systematic advection and subsequent enhanced turbulence at minor topographical features, and that part of the (smaller scale) excess transport at these locations is discernible in EC measurements. During the daytime, this might occur due to heterogeneities in airflow in the surface layer resulting in $\bar{w} > 0$ at some locations. Transport due to $\bar{w} > 0$ is not measured by EC systems but it is likely that at such a position, turbulent transport is also increased, and so the detection of differences to the main tower system, which was situated at a relatively homogeneous spot, would be possible with EC measurements. At night, the fact that the surface layer is stable means that advection may be associated with drainage flows, which could all occur below the EC measurement height. When turbulence resumes at some later time, all the transport may be turbulent without $\bar{w}$ deviating from zero, and could therefore be quantifiable using eddy covariance.

Table 3 details the spatial variation in C at HJP02, comparing C measured by the auxiliary and main systems during the same period using the OLS method. C at the location of the auxiliary system is considered to be different to the main tower location if the mean of the slope of the regression of the auxiliary system is outside the 95% confidence limits of the slope of the main system. At location 1, values of C for the auxiliary and main systems are the same. At location 2, the auxiliary system appears to achieve better closure than the main system. However, no difference is found if the analysis excludes wind directions with flux footprints that extend outside the clearcut.

Table 3 Energy balance closure (C) as indicated by the regression parameters of the total heat flux T against available energy A for the main and auxiliary systems at the HJP02 site

Location[a]	Site	Slope[b]	Intercept[b] (W m^{-2})	n	R^2	RMSE (W m^{-2})
1	Main	0.89 (0.86, 0.91)	−3.09 (−7.16, 0.99)	252	0.96	21.64
	Auxiliary	0.88 (0.86, 0.91)	−10.46 (−14.40, −6.51)	222	0.97	22.25
2	Main	0.84 (0.79, 0.89)	3.55 (−1.35, 8.45)	155	0.90	24.05
	Auxiliary	0.95 (0.91, 1.00)	−6.31 (−11.88, −0.75)	152	0.92	26.09
	Auxiliary	0.91 (0.83, 0.99)[c]	−7.84 (−18.16, 2.48)[c]			
3	Main	0.82 (0.81, 0.83)	3.00 (1.17, 4.84)	812	0.94	22.11
	Auxiliary	0.74 (0.73, 0.75)	3.10 (1.70, 4.36)	803	0.97	16.19

[a] Location 1: 100 m west of the main tower; location 2: 5 m from the edge at the south-eastern corner of the site; location 3: on top of a dark and large windrow of slash with low albedo (0.11)
[b] 95% confidence bounds are given in parentheses
[c] Slope of T against A for the auxiliary system when wind direction was such that the footprint for the turbulent fluxes was expected to lie entirely within clearcut

Table 4 Regression parameters for the variation in A and T_{EC} between location 3 of the auxiliary system and the main site (data shown in Fig. 7)

	Slope[a,b,c]	Intercept[a,b,c]	n	R^2	RMSE (W m^{-2})
A	1.21 (1.20, 1.22)	−1.39 (−2.87, 0.10)	870	0.98	19.06
T_{EC}	1.07 (1.05, 1.08)	−0.50 (−1.87, 0.86)	870	0.97	17.42

[a] $A_{aux} = \text{Slope} \times A_{main} + \text{Intercept}$
[b] $T_{EC\ aux} = \text{Slope} \times T_{EC\ main} + \text{Intercept}$
[c] 95% confidence bounds are given in parentheses

At location 3, C for the auxiliary system is significantly lower than for the main system. The probable explanation is that the field-of-view of the net radiometer did not represent the footprint of T_{EC}. The albedo of the area corresponding to the field-of-view was lower, and therefore R_{snet} was higher. However, the footprint of T_{EC} did not fall entirely within the slash windrow, and so the high R_n was not representative of the footprint of T_{EC}. Figure 7 elucidates this point, showing that A is 20% higher at location 3 compared to the main location, whereas T_{EC} is only 7% higher. This is consistent with the footprint of T_{EC} falling partly, but not entirely, within the windrow of slash. Thus, it is necessary in a C analysis that the footprints of the respective components of Eq. 1 lie within the same homogenous area. This analysis also indicates that there is no significant difference in C between the main and any of the auxiliary system locations caused by the systematic occurrence of horizontal and/or vertical transport of sensible and latent heat in the surface layer.

4.3.2 Implications for the Occurrence of Random Horizontal and/or Vertical Transport of Surface-Layer Fluxes

Regardless of whether EC measurements are able to quantify the horizontal and/or vertical transport of surface-layer fluxes, its existence would lead to increased variability in T relative to A because the relative magnitude of advected fluxes would be correlated with climatic conditions, which exhibit strong diurnal and seasonal variations. However, this is only valid, if these events occur at small scales and are not exclusively associated with mesoscale events of spatial scales of several kilometres or more. If those locations are random with a varying distance from the tower, and some of the excess transport is discernible by eddy covariance,

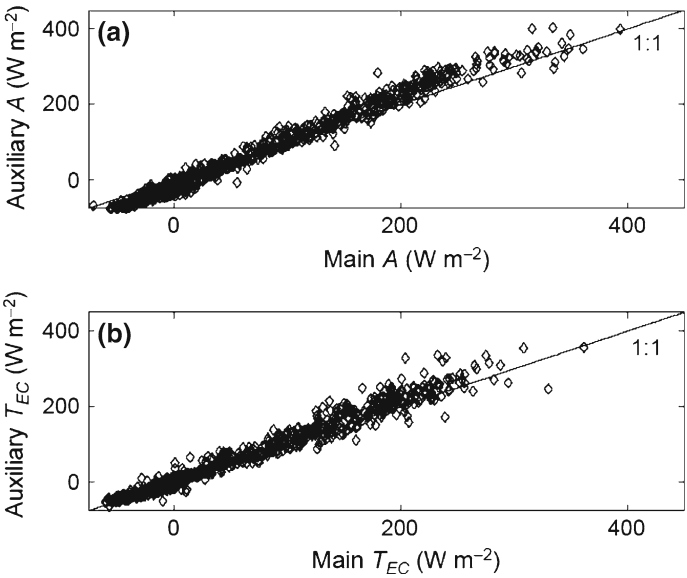

Fig. 7 **a** Regression of A measured by the auxiliary system at location 3 against A measured by the main system at HJP02. **b** Regression of T measured by the auxiliary system at location 3 against T measured by the main system. See Table 4 for regression parameters

the variability of T_{EC} would be further increased. The statistical error of the 95% confidence bounds in the slope for A is ± 0.012, while for T_{EC} it is ± 0.013 when comparing location 3 with the main system (Fig. 7). The same statistical errors when the two systems were side by side are 0.015 and 0.011 for A and T_{EC}, respectively. Separating the two systems does not significantly increase the scatter in T_{EC}, and, moreover, T_{EC} shows approximately the same scatter as A. This result implies that at any one point in time, T_{EC} is well adjusted over a spatial scale on the order of the clearcut and so randomly located horizontal and/or vertical transport of surface-layer fluxes likely did not occur at HJP02. Further evidence to support this conclusion is that the coefficients of determination given in Table 3 are regularly >0.90, which implies that the variation in T is almost completely determined by the variation in A, and is therefore temporally well behaved.

If the measurement period is sufficiently long, the location of horizontal transport events would be expected to coincide with the tower location. In a dataset of many half-hour periods, T_{EC} would therefore be positively skewed relative to A, as it would sometimes be very high. Figure 8 shows the skewness calculated for fluxes at OJP and HJP02 after they were first binned by time of day. The systematic diurnal variation in skewness that is observed in R_{sd}, A and T_{EC} in Fig. 8 is expected because of the seasonal variation in R_{sd}. The same pattern is observed in the skewness of R_{pot}. The skewness of R_{sd} is included as a reference for the 'base' skewness. Figure 8a shows that the skewness of T_{EC} at OJP is systematically higher than the skewness of A. It remains unclear whether this is an artefact of the insufficient averaging time (see Sect. 4.2.2), or whether it is indicative of the existence of horizontal transport locations at OJP. Figure 8b shows that the skewness of T_{EC} at HJP02 is similar to the skewness of A. Therefore, turbulent fluxes are temporally well behaved and provide further evidence that randomly located points of horizontal transport likely did not occur at HJP02.

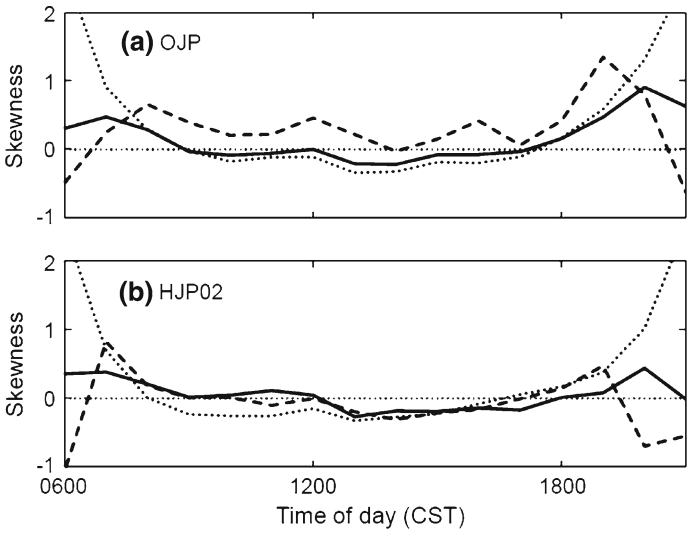

Fig. 8 Diurnal variation of skewness: A (*solid line*), T_{EC} (*dashed line*), and R_{sd} (*dotted line*) at OJP (**a**) and HJP02 (**b**). Skewness was calculated from half-hourly flux values for each hour of the day, i.e., fluxes were first binned by hour of the day, and then the skewness was calculated for the distribution of all the fluxes within a given hour. Data were recorded during daylight hours ($R_{sdpot} > 0$) between May and October 2004 and 2005

4.4 Similarity of Surface-Layer Fluxes

Figure 9 shows a light response curve for OJP data stratified by the closure C. The observations were made during summer, when the downwelling photosynthetic photon flux density (Q_{pd}) was expected to be the main driver of NEE, i.e., when the temperature was above 5°C, and there was no water stress on the trees. During this period there was no seasonal trend in C, which if coupled with the seasonal trend in F_C, mainly produced the results seen in this curve. This light response curve stratified by C shows that during daytime ($Q_{pd} > 0$), for a given level of Q_{pd}, the magnitude of F_C is reduced when C is low. The values of F_C for $Q_{pd} = 0$ show that during nighttime the magnitude of F_C is also reduced during periods of low C. When measured NEE is plotted instead of F_C, the same pattern is observed. Thus, the reduction in the magnitude of F_C during low C periods is not compensated for by S_{CO_2}. Furthermore, the behaviour is not explained by the diurnal covariance of F_C and C, because for $Q_{pd} > 500\,\mu mol\,m^{-2}\,s^{-1}$, there is no diurnal covariance of C and F_C. Figure 9 implies that the fraction of NEE that is measured as F_C is dependent on C. This is consistent with the hypothesis that the variation in C is caused by the measurement of T_{EC}, and that F_C is affected in a qualitatively similar way.

Approximate quantitative similarity is indicated by the fact that for $Q_{pd} > 400\,\mu mol\,m^{-2}\,s^{-1}$, C using the MOR method is 53, 75 and 102% for the low, medium and high C stratifications, respectively, and that the ratio of the mean of F_C for the low and medium stratifications to the mean of F_C for the high stratification is 0.42 and 0.74, respectively. Further quantitative insight into the similarity between the surface-layer fluxes can be gained by restricting the analysis to periods that have similar climatic conditions and investigating how the magnitudes of A, H_{EC}, λE_{EC} and F_C vary together as C varies. Half-hour periods were deemed to be similar when $Q_{pd} > 900\,\mu mol\,m^{-2}\,s^{-1}$, $8 < T_a < 18$°C and $0.07 < VWC < 0.20$,

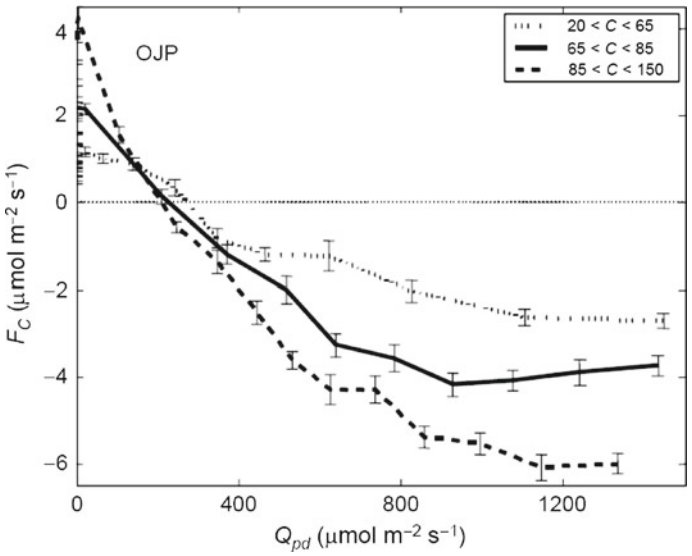

Fig. 9 F_C as a function of downwelling photosynthetic photon flux density (Q_{pd}). Data were recorded at OJP during summer 2004 and have been bin averaged and stratified by C. C during daytime ($Q_{\mathrm{pd}} > 0$) using the MOR method was 53, 75, and 102% for the low, medium, and high C stratifications, respectively. Also shown is the standard error of the mean for each bin

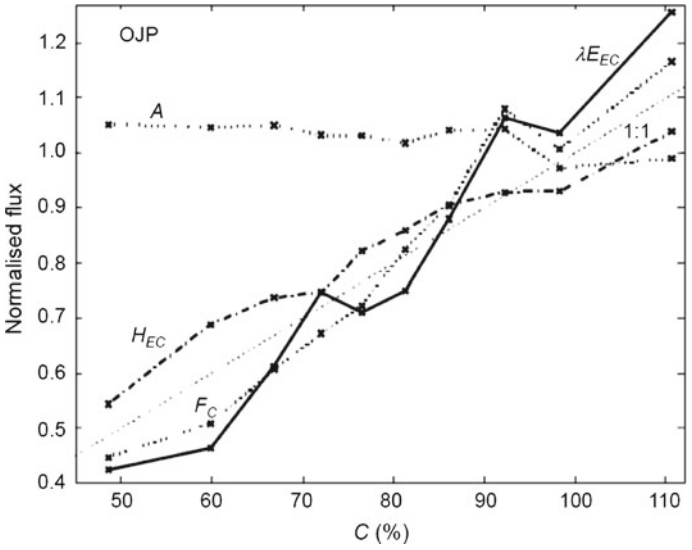

Fig. 10 Normalised fluxes plotted against C: A (*dashed line*), H_{EC} (*dot-dashed line*), λE_{EC} (*solid line*), and F_C (*dotted line*) were normalized by their respective means when $0.98 < C < 1.02$. Data were recorded at OJP when $Q_{\mathrm{pd}} > 900\,\mu\mathrm{mol\,m^{-2}\,s^{-1}}$, $8 < T_a < 18°\mathrm{C}$ and $0.07 < \mathrm{VWC} < 0.2$ during 2003–2005, and have been bin averaged with 150 half-hour periods in each bin

as these measurements are independent of the measurements of A, T_{EC}, and F_C. Figure 10 shows A, H_{EC}, λE_{EC}, and F_C for these half-hour periods for the OJP site during the summers of 2003–2005, all normalized by their respective values at $C = 100\%$. A does not covary with C, and there is an approximately linear relationship between all three EC fluxes and C.

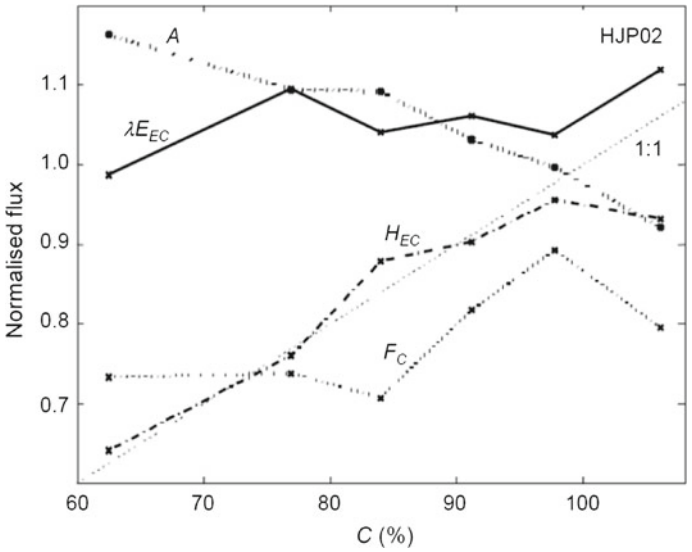

Fig. 11 Normalised fluxes plotted against C: A (*dashed line*), H_{EC} (*dot-dashed line*), λE_{EC} (*solid line*) and F_C (*dotted line*) were normalized by their respective means when $0.98 < C < 1.02$. Data were recorded at HJP02 when $Q_{\mathrm{pd}} > 900\,\mu\mathrm{mol\,m^{-2}\,s^{-1}}$, $8 < T_a < 18°C$ and $0.07 < \mathrm{VWC} < 0.16$ during 2003–2005, and have been bin averaged with 200 half-hour periods in each bin

When the respective storage terms are included in the surface-layer fluxes the same pattern is observed (not shown). The fact that the normalized values of H and λE are correlated with C whereas A is independent of C implies that H and λE cause the variations in C. A similar analysis of the normalized values of Q_{pd}, T_a, and VWC show them to be constant, independent of C, which lends further weight to the conclusion that the half-hour periods shown in Fig. 10 are indeed, on average, similar, and make it extremely unlikely that the variation in C is caused by the accuracy in the measurement of A.

Figure 10 provides strong evidence that (a) the variations in C in the OJP dataset are due to the variations in the ratio of T_{EC}/T, and (b) the variation in T_{EC}/T is controlled by a process that has both a qualitatively and quantitatively similar impact on all of the turbulent fluxes. Regardless of whether this process is entirely related to the insufficient averaging time employed at the OJP site or is also related to the systematic advection of surface-layer fluxes, the data in Fig. 10 corroborate the results of the spectral analysis in Sect. 4.2.2. Despite this finding, forcing T_{EC} to closure while retaining the measured Bowen ratio cannot be justified as it remains uncertain to what extent long wavelength contributions influence the relationship between T_{EC}, F_C and C.

Figure 11 shows a similar analysis for the HJP02 site. As was the case for the OJP site, Q, T_a, and VWC are independent of C, thus eliminating meteorological causes from the patterns in Fig. 11. In contrast to OJP, A is not constant but has a weak (negative) dependence on C, which is consistent with the hypothesis that a variation in A causes at least part of the variation in C. λE_{EC} is relatively constant, and H_{EC} falls close to the 1:1 line. It is possible that this behaviour is entirely explained by the underestimation in λE_{EC}. Figures 3a and 5 show that λE_{EC} is underestimated at HJP02 due to instrumentation issues. Thus, C is lower when the Bowen ratio is low due to the combined effects of λE_{EC} being a large fraction of the energy balance and such half-hour periods tending to occur when relative humidity is high. Therefore, the high-frequency degradation of λE_{EC} is more pronounced. If T were constant for the half-hour periods shown in Fig. 11, then any decrease in H would be balanced by a

corresponding increase in λE. If the hypothesized increase in λE were not measured, then the behaviour displayed in Fig. 11 would be expected. The fact that F_C is relatively constant may be a reflection of F_C being correctly measured throughout these similar half-hour periods.

Our analysis indicates that the variation in C at the HJP02 site is due to the instrumentation performance affecting both A and λE_{EC}. This, combined with the fact that we did not observe similarity between F_C and T_{EC}, serves as a further indication that at least at small scales within the site vertical or horizontal advection of surface-layer fluxes did not occur at HJP02. Furthermore, the results in Sect. 4.2.1 show that the wT_a cospectra fall to zero at both low and high frequencies. Hence, it seems likely that the only underestimation of surface-layer fluxes is due to instrumentation issues, leading to a high-frequency degradation of λE_{EC} and F_C. Only these errors should be taken into account when determining the surface-layer fluxes, thereby assuming that the remaining imbalance is due to the overestimation of A and possibly due to long wavelength contributions of a yet unknown extent.

5 Conclusions

Our study analyzes the closure of the energy balance by the EC technique in a mature forest and an extensive clearcut. Unfavourable mounting of net radiometers likely led to errors in available energy A. Thus, rigorous quantification of the error in the net radiation R_n, including the influence of the tower, is necessary. This needs to be done on a site-by-site basis, accounting for varying instrumentation and tower geometry.

The latent heat flux λE_{EC} was underestimated at the clearcut site due to high-frequency attenuation of the water vapour mixing ratio m_w by the sample tube of the closed-path IRGA. The error this produced in the energy balance closure C is correlated with the NEE because: (i) the error increases when relative humidity is high, and relative humidity is correlated with R_{sd}, which affects NEE; and (ii) the importance of the error depends on the Bowen ratio, which varies with soil moisture, which also affects NEE. Hence, NEE is biased if the surface-layer fluxes are forced for closure and the error in λE_{EC} is assumed to be constant.

Loss of low-frequency covariance due to an insufficient averaging time (30 min) is a significant issue at the OJP site but not at the HJP02 site. Averaging times that are long enough to capture all of the low-frequency covariance at OJP during periods when conditions were relatively stationary appear to be too long to accurately resolve all of the high-frequency covariance when conditions were non-stationary. Also, the shorter averaging times during these non-stationary conditions are insufficient to capture all of the low-frequency covariance, raising the possibility that eddy covariance cannot accurately quantify ecosystem–atmosphere exchange during such conditions.

The closure analysis differed between sites. At OJP, analysis of the relative magnitudes of the surface-layer fluxes during similar half-hour periods (that exhibit a range of closure) shows that the variation in closure is due to the underestimation in the measurement of T and the result of micrometeorological processes that affect H, λE and NEE in a qualitatively, but not necessarily in a quantitatively, similar way. Therefore, forcing T_{EC} to closure while retaining the measured Bowen ratio, and applying the same factor to F_C, cannot be firmly recommended on the basis of this study, as it remains unclear as to what extent long wavelength contributions influence the relationship between T_{EC}, F_C and C.

At HJP02, the surface-layer fluxes were temporally and spatially well behaved, indicating that systematic horizontal or vertical transport away from the EC tower did not occur at the site. Furthermore, analysis of the relative magnitudes of the surface-layer fluxes during similar half-hours indicates that variations in closure are not due to micrometeorological

processes that affect all three surface-layer fluxes similarly, and therefore the surface-layer fluxes should not be forced for closure.

Acknowledgements Funding was provided by the Canadian Carbon Program (CCP) formerly Fluxnet Canada Research Network (FCRN) through Natural Sciences and Engineering Research Council of Canada (NSERC), the Canadian Foundation for Climate and Atmospheric Sciences (CFCAS) and BIOCAP Canada, a NSERC operating grant to Andy Black, and also the Climate Research Branch of Environment Canada. Scientific advice by R. Stull and T. Oke was much appreciated. The technical assistance of Andrew Sauter, Rick Ketler, Shawn O'Neill and Stephanie Thompson is sincerely acknowledged, as is the maintenance and quality assurance of meteorological measurements provided by Werner Bauer, Dell Bayne, Natasha Neumann, Erin Thompson, Steve Enns, Dave Wieder, and help provided by David Gaumont-Guay and Iain Hawthorne.

References

Aubinet M, Grelle A, Ibrom A, Rannik U, Moncrieff J, Foken T, Kowalski AS, Martin PH, Berbigier P, Bernhofer C, Clement R, Elbers J, Granier A, Grünwald T, Morgenstern K, Pilegaard K, Rebmann C, Snijders W, Valentini R, Vesala T (2000) Estimates of the annual net carbon and water exchange of forests: the EUROFLUX methodology. Adv Ecol Res 30:113–176

Baldocchi D (2003) Assessing the eddy covariance technique for evaluating carbon dioxide exchange rates of ecosystems: past, present and future. Glob Change Biol 9:479–492

Baldocchi D (2008) 'Breathing' of the terrestrial biosphere: lessons learned from a global network of carbon dioxide flux measurement systems. Aust J Bot 56:1–26

Baldocchi D, Vogel CA, Hall B (1997) Seasonal variation of carbon dioxide exchange rates above and below a boreal jack pine forest. Agric For Meteorol 83:147–170

Barr AG, Morgenstern K, Black TA, McCaughey JH (2006) Surface energy balance closure by the eddy-covariance method above three boreal forest stands and implications for the measurement of the CO_2 flux. Agric For Meteorol 140:322–337

Black TA, Den Hartog G, Neumann HH, Blanken PD, Yang PC, Russell C, Nesic Z, Lee X, Chen SG, Staebler R, Novak MD (1996) Annual cycles of water vapour and carbon dioxide fluxes in and above a boreal aspen forest. Glob Change Biol 2:219–229

Blanken PD, Black TA, Neumann HH, Den Hartog G, Yang PC, Nesic Z, Staebler R, Chen W, Novak MD (1998) Turbulent flux measurements above and below the overstory of a boreal aspen forest. Boundary-Layer Meteorol 89:109–140

Campbell GS, Norman JM (1998) An introduction to environmental biophysics. Springer, New York, 286 pp

Chen JM, Govind A, Sonnentag O (2006) Leaf area index measurements at Fluxnet-Canada forest sites. Agric For Meteorol 140:257–268

Finnigan J (1999) A comment on the paper by Lee (1998): on micrometeorological observations of surface–air exchange over tall vegetation. Agric For Meteorol 97:55–64

Finnigan J, Clement R, Mahli Y, Leuning R, Cleugh HA (2003) A re-evaluation of long-term flux measurement techniques. Part I: averaging and coordinate rotation. Boundary-Layer Meteorol 107:1–48

Griffis TJ, Black TA, Morgenstern K, Barr AG, Nesic Z, Drewitt GB, Gaumont-Guay D, McCaughey JH (2003) Ecophysiological controls of the carbon balance of three southern boreal forests. Agric For Meteorol 117:53–71

Kanda M, Inagaki A, Letzel MO, Raasch S, Watanabe T (2004) LES study of the energy imbalance problem with eddy covariance fluxes. Boundary-Layer Meteorol 110:381–404

Kljun N, Rotach MW, Schmid HP (2002) A three-dimensional backward Lagrangian footprint model for a wide range of boundary-layer stratifications. Boundary Layer Meteorol 103:205–226

Kljun N, Black TA, Griffis TJ, Barr AG, Gaumont-Guay D, Morgenstern K, McCaughey JH, Nesic Z (2006) Response of net ecosystem productivity of three boreal forest stands to drought. Ecosystems 9:1128–1144

Law BE, Falge E, Gu L, Baldocchi D, Bakwin P, Berbigier P, Davis K, Dolman AJ, Falk M, Fuentes JD, Goldstein A, Granier A, Grelle A, Hollinger D, Janssens IA, Jarvis P, Jensen NO, Katul G, Mahli Y, Matteucci G, Meyers T, Monson R, Munger W, Oechel W, Olson R, Pilegaard K, Paw U KT, Thorgeirsson H, Valentini R, Verma S, Vesala T, Wilson K, Wofsy S (2002) Environmental controls over carbon dioxide and water vapor exchange of terrestrial vegetation. Agric For Meteorol 113:97–120

Lee X (1998) On micrometeorological observations of surface-air exchange over tall vegetation. Agric For Meteorol 91:39–49

Lee X, Black TA (1993) Atmospheric turbulence within and above a Douglas-fir stand. 1. Statistical properties of the velocity-field. Boundary-Layer Meteorol 64:149–174

Liu H, Randerson JT, Lindfors J, Massman WJ, Foken T (2006) Consequences of incomplete surface energy balance closure for CO_2 fluxes from open-path CO_2/H_2O infrared gas analysers. Boundary-Layer Meteorol 120:65–85

Mahrt L (1998) Flux sampling errors for aircraft and towers. J Atmos Ocean Technol 15:416–429

Massman WJ (2000) A simple method for estimating frequency response corrections for eddy covariance systems. Agric For Meteorol 104:185–198

Massman WJ, Lee X (2002) Eddy covariance flux corrections and uncertainties in long-term studies of carbon and energy exchanges. Agric For Meteorol 113:121–144

Mauder M, Desjardins RL, Oncley SP, MacPherson JI (2007) Atmospheric response to a solar eclipse over a cotton field in Central California. J Appl Meteorol Clim 46:1792–1803

McNaughton KG (2004) Turbulence structure of the unstable atmospheric surface layer and transition to the outer layer. Boundary-Layer Meteorol 112:199–221

Schmid HP (1994) Source areas for scalars and scalar fluxes. Boundary-Layer Meteorol 67:293–318

Stull RB (1998) Introduction to boundary layer meteorology. Kluwer, Dordrecht, 666 pp

Tanner CB, Thurtell GW (1969) Anemoclinometer measurements of Reynolds stress and heat transport in the atmospheric surface layer. ECOM 66-G22-F, University of Wisconsin, Madison, Wisconsin, pp 61–72

Twine TE, Kustas WP, Norman JM, Cook DR, Houser PR, Meyers TP, Prueger JH, Starks PJ, Wesely ML (2000) Correcting eddy-covariance flux underestimates over a grassland. Agric For Meteorol 103:279–300

Wilson K, Goldstein A, Falge E, Aubinet M, Baldocchi D, Berbigier P, Bernhofer C, Ceulemans R, Dolman H, Field C, Grelle A, Ibrom A, Law BE, Kowalski A, Meyers T, Moncrieff J, Monson R, Oechel W, Tenhunen J, Valentini R, Verma S (2002) Energy balance closure at FLUXNET sites. Agric For Meteorol 113:223–243

Wofsy SC, Goulden ML, Munger JW, Fan SM, Bakwin PS, Daube BC, Bassow SL, Bazzaz FA (1993) Net exchange of CO_2 in a mid-latitude forest. Science 260:1314–1317

Zha T, Barr AG, Black TA, McCaughey JH, Bhatti J, Hawthorne I, Krishnan P, Kidston J, Saigusa N, Shashkov A, Nesic Z (2009) Carbon sequestration in boreal jack pine stands following harvesting. Glob Change Biol 15:1475–1487